DOI: 10.13009/EUCASS2019-400

The Research of the Application of Spatial Interpolation Methods in the Two-Body Proximity Test Data of TSTO

Feng XIE, Guanxin HONG***

** School of Aeronautic Science and Engineering, Beihang University, China; China Academy of Aerospace Aerodynamics, China*

NO.17, Xungun West Road, Fengtai District, Beijing. xiefeng11112@163.com

*** School of Aeronautic Science and Engineering, Beihang University, China*

NO.37, Xueyuan Road, Haidian District, Beijing. honggx@buaa.edu.cn

Abstract

Reusable space vehicle is an important research area for the supersonic and hypersonic technology in the future, in which the Two-Stage-To-Orbit (TSTO) is the most accessible scheme at the present stage..One key technology required by TSTO is the acquisition and analysis of the stage separation aerodynamic characteristic. At present, the cognition of the complicated aerodynamic interference phenomenon in the supersonic and hypersonic parallel stage separation is lack of depth and comprehensiveness.. In this paper, the single-body test and two-body proximity test of a TSTO configuration are initiated at Ma3 condition in the FD12 wind tunnel of the China Academy of Aerospace Aerodynamics.. The test data shows that the longitudinal and vertical separation have a non-linear influence on the stage-separation aerodynamic coefficients.. Four spatial interpolation methods, ordinary kringing method, inverse distance weighting method, spline method and polynomial regression method, are employed to study the establishment of the aerodynamic interference model under the coupling of the longitudinal and vertical separation.. The interpolation accuracy indexes are used to evaluate the feasibility and effectiveness of the four spatial interpolation methods. Finally, the spatial interpolation method which is most suitable for the TSTO two-body proximity test data is determined, which can effectively support the subsequent analysis and processing of a large number of test data.

1. Introduction

Reusable space vehicle is an effective way to reduce the cost of spaceflight transportation, and is an important research area for the supersonic and hypersonic technology in the future. in which the Two-Stage-To-Orbit (TSTO) is the most accessible scheme at the present stage. Many countries, have been studying the reusable space vehicles in order to meet the needs of the future launch vehicles, which are cheaper, safer and more reliable [1-5]. In the TSTO stage parallel separation process, the complex aerodynamic interferences such as shock wave-shock wave interaction, shock wave-boundary layer interaction exist in the flow field. The establishment of the aerodynamic model is an important part for the study of the aerodynamic interference, and is also an important basis for the study of the two-stage separation trajectory and safety separation criterion. The establishment method for the aerodynamic model of TSTO parallel stage separation is in urgent need.

Many experts have been studying the establishment method of the aerodynamic model for aircrafts. In order to directly reflect the relation between the aerodynamic coefficient and the influence factors, Polynomial regression model is widely used to establish the aerodynamic model. Morelli proposed the multivariate orthogonal function method to obtain the global model of the longitudinal aerodynamic coefficients of F-16 fighter [6]; Visser et al. proposed a method based on the multivariate spline function to construct the aerodynamic coefficient model [7]; Sun L G proposed a sequential recursion method based on multivariate spline function which can be used to build the online aerodynamic model [8]； Pamadi proposed the multivariate interpolation coefficient method which can be used to obtain the global model of longitudinal aerodynamic coefficient of LGBB two-stage orbiting vehicle [9]. The polynomial regression model has been successfully used to establish the linear aerodynamic model. However, when it is used to establish the complicated nonlinear aerodynamic model, the unacceptable fit error exists [10,11].

As the aerodynamic characteristic during the TSTO parallel separation process is nonlinear and multivariable coupled, it is difficult to obtain and analyze the stage separation aerodynamic characteristic . In this paper, the single-body wind tunnel test and two-body proximity wind tunnel test of TSTO are carried out, and the influential factors

DOI: 10.13009/EUCASS2019-400

on the separation aerodynamic force and moment are studied and analyzed. Four spatial interpolation methods are used to establish the nonlinear aerodynamic interference model. The interpolation accuracy indexes are used to evaluate the advantages and disadvantages of the four spatial interpolation methods in the application of the TSTO supersonic parallel separation aerodynamic data, based on which the spatial interpolation method with stronger applicability is selected.

2. Single-body test and two-body proximity test of TSTO

In order to study the influential factors of the TSTO aerodynamic interference, single-body test and two-body proximity test of TSTO are needed to be carried out to acquire the non-inference aerodynamic data and with-interference aerodynamic data.

2.1 Design of the wind tunnel test

According to the typical characteristics of TSTO, the research model of the TSTO is shown in Figure 1.

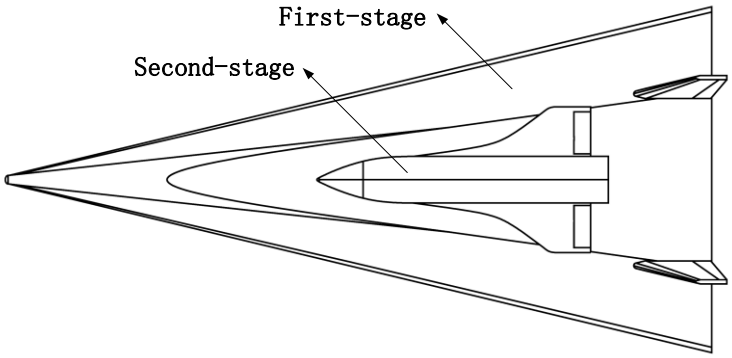

Figure 1: The diagram of the first-stage model and second-stage model for TSTO

The single-body test for the first-stage model, single-body test for the second-stage model and the two-body proximity test were carried out in the FD-12 wind tunnel of China Academy of Aerospace Aerodynamics. The parameters of the flow field are shown in Table 1.

Table 1: The parameter of the flow field

MA	P0(Pa)	P(Pa)	q8(Pa)	Re($\times 10^6$ 1/m)
3	198099	5393	33976	17.09

In the single-body test for the first-stage model, the attack angle range is -8 ~ 2 °. In the single-body test for the second-stage model, the attack angle range is-12 ~ 12 °.

In the two-body proximity test, the first-stage model is supported by a angle-of-attack mechanism, and the second-stage model is supported by a six-degree-of-freedom mechanism. The variables in the two-body proximity test include: the relative longitudinal position, the lateral position and the relative angle of attack. The first-stage model is fixed with α_1=0 °. In the condition of *Ma*=3, a shock wave with Mach angle λ=19.47° is generated at the nose of the first-stage model. The relative position *X*, position *Z* and attack angle α_2 are set around the shock wave, as shown in Figure 2. The *X* and *Y* are expressed by the ratio relative to the reference length *L* of the two-stage model.

Range of *X* (/*L*)：-0.2，0，0.2，0.4，0.6

Range of *Z* (/*L*)：0，0.1，0.2，0.3，0.45，0.65

Range of α_2 (°)：-5，0，5

DOI: 10.13009/EUCASS2019-400

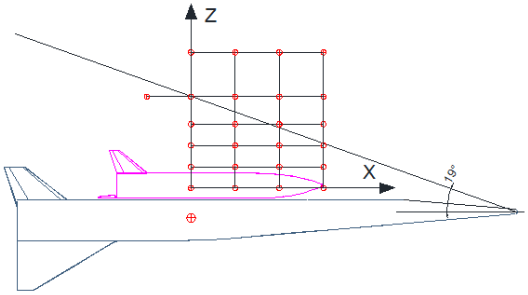

Figure 2: Design of grid points for the two-body proximity test

2.1 Test results and analysis

Based on the *X* position influence and the *Z* position influence on the aerodynamic interference, the test results and analysis are divided into two parts.

(1) The influence of *X* positions on the aerodynamic force of the second-stage model

The selected grid points obviously reflecting the *X* position influence are shown as the frame area in Figure 3. The horizontal positions of the five points in this area are: *X*(/*L*) = -0.2, 0, 0.2, 0.4, 0.6. The centroid of the second-stage model is designed on the shock surface at the position of *X*(/*L*)=0, and it is behind the shock surface at the position of *X*(/*L*)=-0.2, and it is in front of the shock wave at the positions of *X*(/*L*)=0.2, 0.4, 0.6. The influence of the shock wave generated by the first-stage model on the second-stage model can be investigated by the different *X* positions with different shock wave-shock wave, shock wave-boundary layer interferences. The comparison of the pitch moment coefficient *Cmz* and the nominal force coefficient *CN* between the single-body test and two-body proximity test with the different *X* positions is shown in Figure 4.

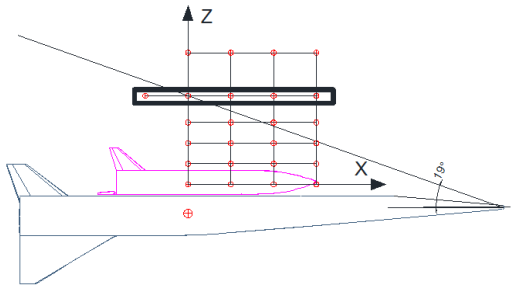

Figure 3: Mesh points at different X position

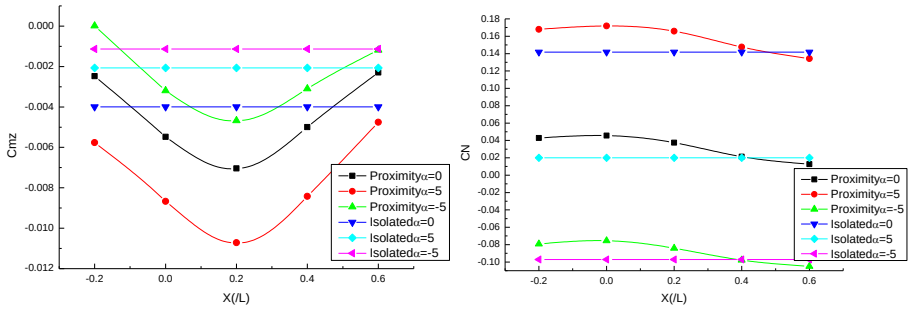

Figure 4: Comparison of *Cmz* and *CN* between the single-body test and two-body proximity test with the different *X* positions

It can be derived from Figure 4：

（a）The pitch moment *Cmz* of the second-stage model at *X*(/*L*)=-0.2 reaches the minimum value, and it approximately symmetrically grows along the *X* axis; When *X*(/*L*)=0.6, *Cmz* is approximately equal to that of the single-body test, indicating that the pitch moment is almost undisturbed; When *X*(/*L*)=-0.2, the number of Mach after the shock surface decreases slightly, and the *Cmz* here is slightly different from that of the single-body test.

（b）The normal force coefficient *CN* at *X(/L)*=-0.2, 0 and 0.2 are slightly higher than the *CN* of the single-body test, and the *CN* at *X*(/*L*)=0.4 and 0.6 are almost the same as the *CN* for the single-body test.

（2）The influence of *Z* positions on the aerodynamic force of the second-stage model

The selected points are shown as the frame area in Figure 5, and the vertical positions of the second-stage model are: *Z(/L)*= 0, 0.1, 0.2, 0.3, 0.45, 0.65. The centroid of the second-stage model at *Z(/L)*=0.45 is designed on the shock

DOI: 10.13009/EUCASS2019-400

surface, the point at *Z(/L)*=0.65 is outside the shock surface and the other four points are inside the shock surface. Among the selected points, the variation of *Cmz* and *CN* for the second-stage model can be investigated when crossing the shock surface vertically. The comparison of *Cmz* and *CN* between the single-body test and two-body proximity test with the different *Z* positions is shown in Figure 6.

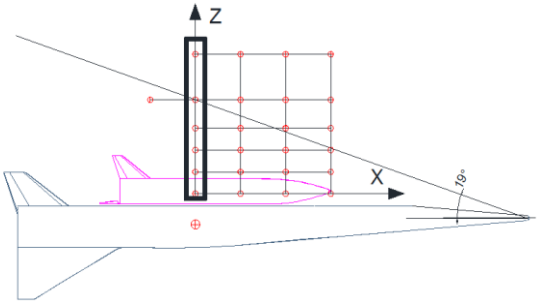

Figure 5: Mesh points at different Z position

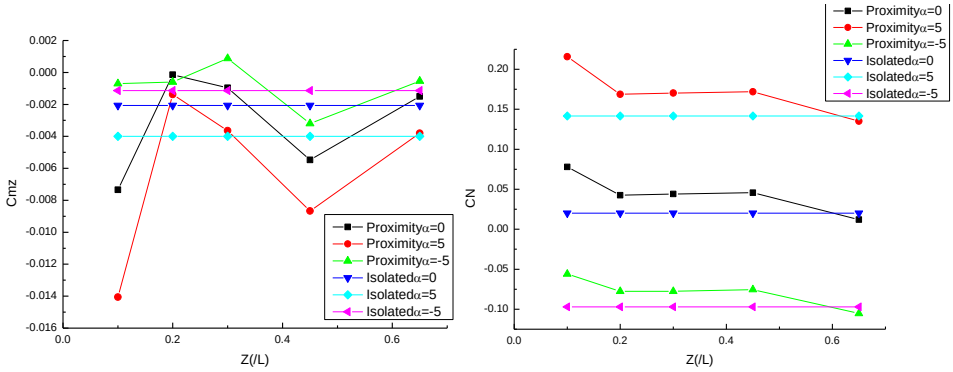

Figure 6: Comparison of *Cmz* and *CN* between the single-body test and two-body proximity test with the different *Z* positions

It can be derived from Figure 6：

Among the points at *Z(/L)*= 0, 0.1, 0.2, 0.3, 0.45, the *Cmz* decreases rapidly to nose-down moment and fluctuates up and down compared to the *Cmz* line of the single-body test, and the *CN* is slightly higher than that of the single-body test.

When the point is at *Z(/L)*=0.65, the *Cmz* and the *CN* of the two-body proximity test are almost equal to those of the single-body test.

As shown in the Figure 4 and Figure 6, it also can be seen that the attack angle has little influence on the aerodynamic interference. In the two-body proximity test, the aerodynamic interference has nonlinear characteristics with *X* positions and *Z* positions. Therefore, when employing the spatial interpolation method to establish the aerodynamic interference model, the *X* positions and *Z* positions are considered as the main influencing factor.

3. The application of the spatial interpolation method

3.1 Spatial interpolation method

3.1.1 Ordinary Kringing

The Ordinary Kringing (OK) is based on the theory of regional variation. The optimal weight coefficient and the optimal estimate are obtained by the semi-variant function [12]. The selection of the variation model determines the optimal weight coefficient, and the selection of the weight coefficient determines the accuracy of the estimation.. In this paper, the spherical function model is selected as the variation model. The calculation equation of Ordinary Kringing is as follows:

$$Z\left(x_0\right)=\sum_{i=0}^{n}\lambda_i Z\left(x_i\right) \tag{1}$$

Where, x_i is the point of the given value, x_0 is the point of the estimate value, $Z\left(x_0\right)$ is the estimate value at the point of x_0, $Z\left(x_i\right)$ is the given value at the point of x_i, n is the amount of sample points, λ_i is the weight coefficient.

DOI: 10.13009/EUCASS2019-400

3.1.2 Inverse Distance Weighting

The theoretical basis of Inverse Distance Weighting (IDW) is the similarity principle, that is, the closer the distance between the two points in space is , the smaller the spatial difference is. Inverse Distance Weighting calculates the distance between the given-data points and the estimated-data points, and performs the weighted average calculation to get the estimated values. The calculation equation of Inverse Distance Weighting is as follows:

$$\lambda_i = \frac{d_i^{-p}}{\sum_{i=0}^{n} d_i^{-p}} \quad \sum_{i=0}^{n} \lambda_i = 1 \tag{2}$$

Where, p is the exponent, d_i is the distant between the estimated-data point to the given-data point.

3.1.3 Spline

Spline is an interpolation method to produce the smooth interpolation curve by polynomial fitting the given-data points [13]. In this paper, the spline function method based on ArcGIS is used to interpolate. The equation is as follows:

$$Z = \sum_{i=1}^{n} \lambda_i R(d_i) + T(x, y) \tag{3}$$

Where, Z is the estimated value, n is the amount of sample points, λ_i is the coefficient, d_i is the distance between the estimated-data point to the given-data point i; x、y is the horizontal and longitudinal coordinate value in the plane Cartesian coordinate system; $R(d_i)$ is a equation with d_i as its variable; $T(x, y)$ is a linear equation with x, y as its variables. The equations of $R(d_i)$ and $T(x, y)$ are as follows:

$$R(d) = \frac{\frac{d^2}{4}\left[\ln\left(\frac{d}{2\pi}\right) + c - 1\right] + \tau\left[k(\frac{d}{\pi}) + c\right] + \ln\left(\frac{\gamma}{\pi}\right)}{2\pi}$$

$$T(x, y) = a_1 + a_2 x + a_3 y$$

Where, τ is the weight coefficient, k is the Bessel function, c is a constant value, $a_1 \sim a_3$ are the coefficients.

3.1.4 Polynomial Regression

According to the sample datas, Polynomial Regression (PR) fits a mathematical surface, which is used to reflect the change of spatial distribution [14]. The equation of the Polynomial Regression method is as follows:：

$$Z(x, y) = \sum_{k=0}^{n_0} \sum_{i}^{k} a_{k,j} k x^{k-i} y^i + \varepsilon \tag{4}$$

Where, $Z(x, y)$ is the estimated value; n_0 is the index of the polynomial ; ε is the random error between the mathematical surface and the actual surface, $a_{k,j}$ is the coefficient, x is the horizontal coordinate value, y is the longitudinal coordinate value.

3.2 Interpolation accuracy evaluation method

The main evaluation indexes of interpolation accuracy are as follows: mean absolute error (MAE), mean relative error (MRE) and root mean square (RMSIE) [15]. MAE can estimate the range of possible estimation errors, MRE generally reflects the value of estimation errors, and RMSIE can reflect the estimation sensitivity and extremum effects of sample data. MAE, MRE and RMSIE are expressed as follows:

$$\mathrm{MAE} = \frac{1}{n}\sum_{i}^{n} \mathrm{ABS}(\hat{r}_i - r_i)$$

$$\mathrm{MAR} = \frac{1}{n}\sum_{i}^{n} \mathrm{ABS}\left(\frac{\hat{r}_i - r_i}{\hat{r}_i}\right)$$

DOI: 10.13009/EUCASS2019-400

$$\mathrm{RMSIE} = \sqrt{\frac{1}{n}\sum_{i}^{n}\left(\hat{r}_i - r_i\right)^2}$$

Where， $\hat{r}_i$ is the given data， r_i is the estimated data， n is the amount of estimated points.

3.3 Interpolation results and analysis

All the two-body proximity test grid points are shown in the Figure 7, which are used as the given-data points when employing the spatial interpolation method. When evaluating the interpolation accuracy, the points in the square frame and the oval frame would been taken away from the given-data points and taken as the estimated-data points.

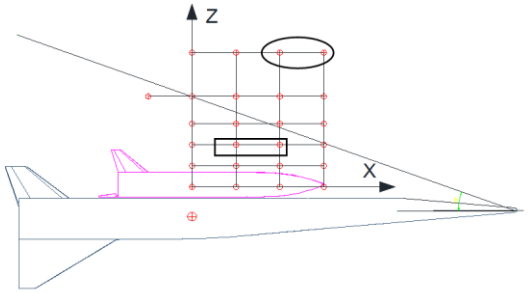

Figure 7: The test grid points

Four spatial interpolation methods, Ordinary Kringing, Inverse Distance Weighting, Spline and Polynomial Regression, are used to interpolate *Cmz*, and *CN* in the X-Z space respectively. The interpolation results are shown in Figure 8 and Figure 9. The evaluation indexes, MAE, MAR and RMSIE, are shown in Figure 10.

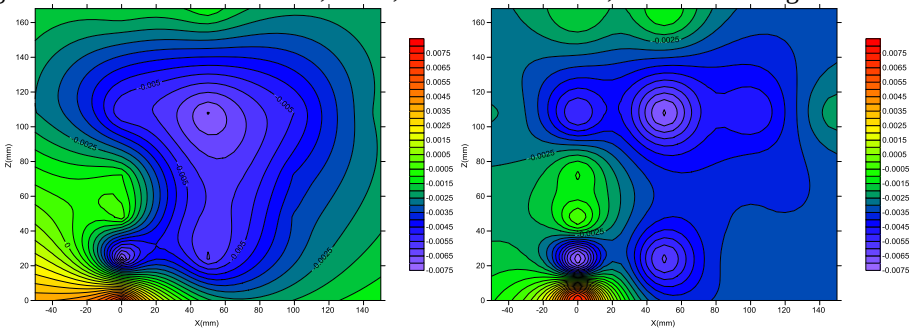

(a) Cloud chart of *Cmz* for Ordinary Kringing (b) Cloud chart of *Cmz* for Inverse Distance Weighting

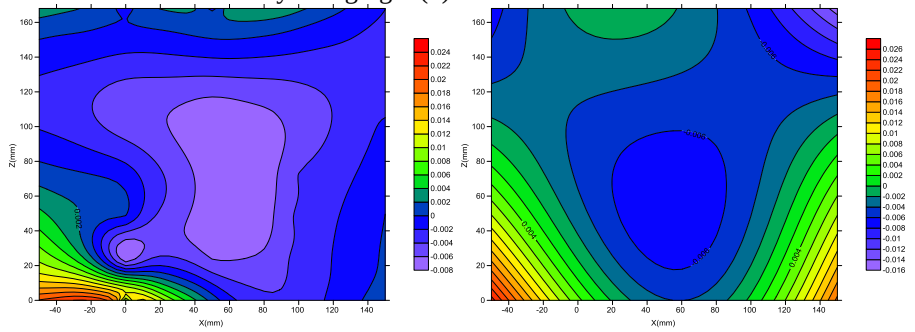

(c) Cloud chart of *Cmz* for Spline (d) Cloud chart of *Cmz* for Polynomial Regression

Figure 8: Cloud chart of *Cmz* for four spatial interpolation methods

DOI: 10.13009/EUCASS2019-400

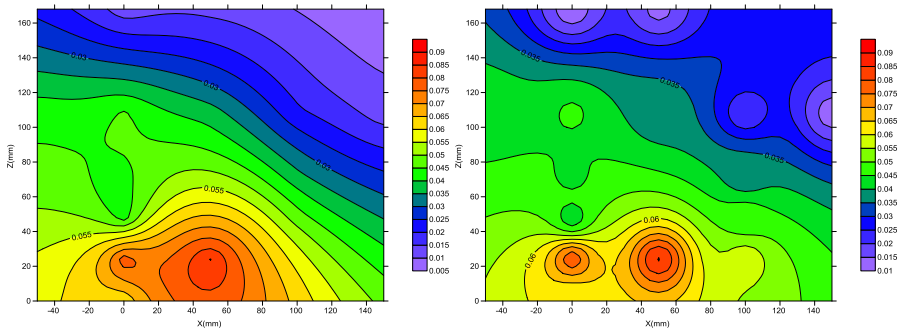

(a) Cloud chart of *CN* for Ordinary Kringing (b) Cloud chart of *CN* for Inverse Distance Weighting

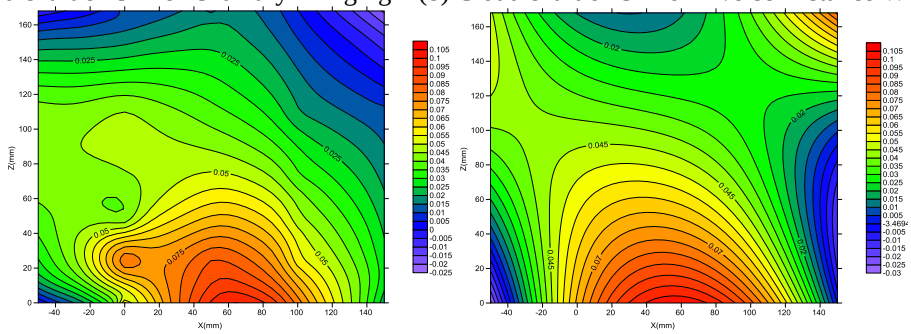

(c) Cloud chart of *CN* for Spline (d) Cloud chart of *CN* for Polynomial Regression

Figure 9: Cloud chart of *CN* for four spatial interpolation methods

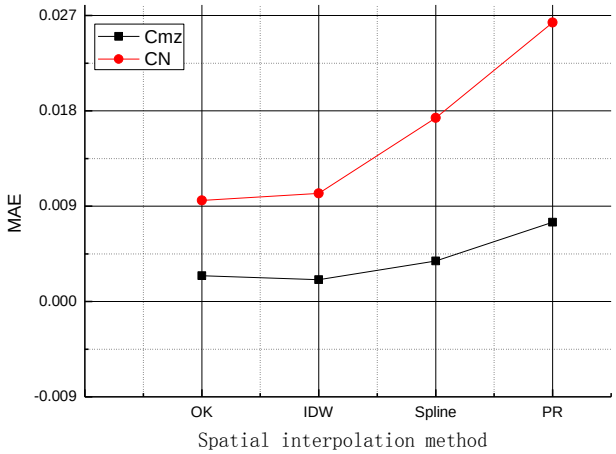

(a) MAE of aerodynamic coefficient for four spatial interpolation methods

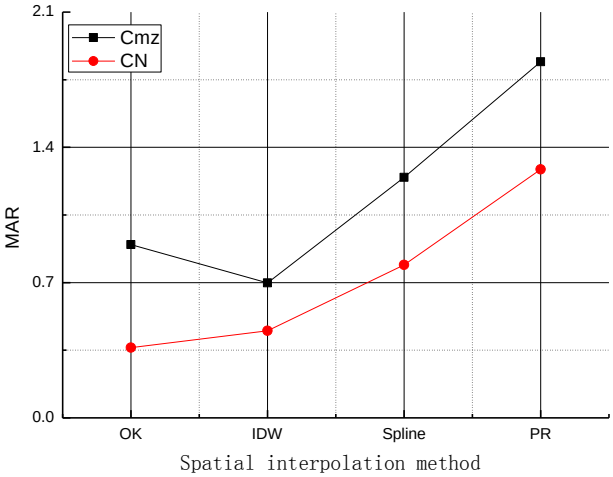

(b) MAR of aerodynamic coefficient for four spatial interpolation methods

DOI: 10.13009/EUCASS2019-400

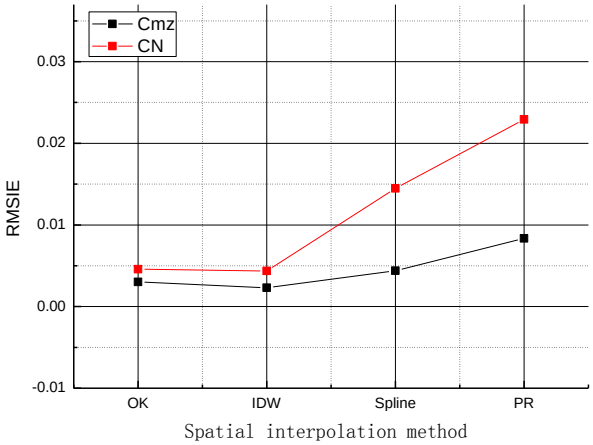

(c) RMSIE of aerodynamic coefficient for four spatial interpolation methods

Figure 10: Comparison of interpolation accuracy

Figure 10 shows that, in the application of TSTO aerodynamic interference interpolation, MAE, MAR, and RMSIE for Ordinary Kringing and Inverse Distance Weighting are obviously better than those for Spline and Polynomial Regression; Ordinary Kringing and Inverse Distance Weighting have the approximately equivalent interpolation accuracy, RMSIE of which is better than 0.005, and both meet the requirement of aerodynamic loading interpolation for TSTO parallel separation.

4. Conclusion

As the unacceptable fit error exists when polynomial regression is used to establish the complicated nonlinear aerodynamic model, spatial interpolation methods are introduced to establishing the aerodynamic interference model for TSTO parallel separation. In this paper, the single-body test and two-body proximity test of TSTO are carried out in the Ma3 flow field of FD12 wind tunnel. Four spatial interpolation methods are used to study the aerodynamic interference model. The four spatial interpolation methods are compared and analyzed with the interpolation precision indexes. The study shows that：

(1) Ordinary Kringing and Inverse Distance Weighting have the approximately equivalent interpolation accuracy in the application of TSTO aerodynamic interference interpolation, which are obviously better than Spline and Polynomial Regression;

(2) The RMSIE of Ordinary Kringing and Inverse Distance Weighting is better than 0.005, which means both the two methods meet the requirement of aerodynamic load interpolation for TSTO parallel separation;

(3) The aerodynamic interference model is mainly affected by the relative positions of two stages.

References

[1] Department of the Air Force, Mission Need Statement for Operationally Responsive Spacelift[J], AFSPC 001-01, HQ AFSPC/DRS, United States Air Force, 20 December 2001, p. 1.

[2] Caceres, M. A., EELV Program Reaches Maturity[J], Military Aerospace Technology, Vol. 2, No. 1, 2 Feb 2003.

[3] Chase, R. and Tang, M., The Quest for Single Stage Earth-to-Orbit: TAV, NASP, DC-X and X-33 Accomplishments, Deficiencies, and Why They Did Not Fly[R] ,AIAA 2002-5143, 11th AIAA/AAAF International Space Planes and Hypersonic Systems Technology Conference, Orleans, France, September 2002.

[4] United States Air Force Scientific Advisory Board, Why and Whither Hypersonics Research in the U. S. Air Force[J], SABTR-00-03, United States Air Force, December 2003, pp. 27-28.

[5] Caldwell, R. A., “Weight Analysis of Two-Stage-to-Orbit Reusable Launch Vehicles for Military Applications,” MS Thesis, AFIT/GA/ENY/05-M02, Graduate School of Engineering and Management, Air Force Institute of Technology (AU), Wright Patterson AFB, OH, March 2005.

DOI: 10.13009/EUCASS2019-400

[6] Morelli E A. Global nonlinear aerodynamic modeling using multivariate orthogonal functions [J]. Journal of Aircraft, 1995, 32(2): 270 -277.
[7] De Visser C C, van Kampen E, Chu Q P, et al. A New Framework for Aerodynamic Model Identification with Multivariate Splines [C]. AIAA Atmospheric Flight Mechanics Conference, 2013
[8] Sun L G, de Visser C C, Chu Q P, et al. Online aerodynamic model identification using a recursive sequential method for multivariate splines[J]. Journal of Guidance, Control, and Dynamics, 2013, 36(5): 1278 -1288.
[9] Pamadi, B. N., et al., Simulation and Analyses of Staging Maneuvers of Next Generation Reusable Launch Vehicles[R], AIAA Paper 2004-5185, August 2004.
[10] Richard Deloach, Erickson Gary. Low-order response surface modeling of wind tunnel data over truncated inference subspaces[R]. AIAA Papar 2003-0456.
[11] Erickson G E. Estimation of supersonic stage separation aerodynamics of winged-body launch vehicles using response surface methods[R]. NASA/TM-2010-216196, 2010.
[12] Dale Z, Claire P, Amy R, et al. An Experimental Comparison of Ordinary and Ordinary and Universal Kringing and Inverse Distance Weighting[J], Mathematical Geology, Vol. 31, Issue 4, 375-390, May 1999.
[13] Amirfakhrian M. Approximation of 3D-Parametric Functions by Bicubic B-spline Functions [J]. Mathematical Modeling & Computations, Vol. 02, No. 03, 211-220, 2012.
[14] Michael J. Z., Raymond F. Z., Zhen Zhang, Multilevel Latent Polynomial Regression for Modeling (in) Congruence Across Organizational Groups[J], The Case of Organizational Culture Research, Vol. 19, Issue 1, 2016.
[15] Chaokui Li, Liang Chen, Yong Wang, et al., On Effects of Weights in Spatial Interpolation[R], Proceeding of the 8th International Symposium on Spatial Accurary Assessment in Natural Resources and Environmental Sciences, 78-84, June 2008.